

A virtual detector approach to tunnel ionization and tunneling times

Nicolas Teeny,^{*} Christoph H. Keitel, and Heiko Bauke[†]

Max-Planck-Institut für Kernphysik, Saupfercheckweg 1, 69117 Heidelberg, Germany

Tunneling times in atomic ionization is studied theoretically by a virtual detector approach. A virtual detector is a hypothetical device that allows to monitor the wave-function's density with spatial and temporal resolution during the ionization process. With this theoretical approach, it becomes possible to define unique moments when the electron enters and leaves with highest probability the classically forbidden region from first principles and a tunneling time can be specified unambiguously. It is shown that neither the moment when the electron enters the tunneling barrier nor when it leaves the tunneling barrier coincide with the moment when the external electric field reaches its maximum. Under the tunneling barrier as well as at the exit the electron has a nonzero velocity in electric field direction. This nonzero exit velocity has to be incorporated when the free motion of the electron is modeled by classical equations of motion.

PACS numbers: 03.65.Xp, 32.80.Fb

1. Introduction

In a seminal work, MacColl [1] studied the time that may be associated with the process of a particle approaching from far away a potential barrier of a height larger than the particle's energy and eventually tunneling through the barrier. A series of subsequent works led to various definitions of tunneling times and different physical interpretations [2–4]. Also many efforts have been directed towards measuring [5–9] tunneling times.

A related still open and actively studied problem of atomic physics is the question how long it takes to ionize an atom via an electron tunneling through the potential barrier [10–27] which is formed by the electron's binding energy and the Coulomb potential bent by the time-dependent electric field's potential, see Fig. 1. Employing the angular streaking technique the tunneling dynamics can be studied on subcycle time scales [13, 14] in the so-called attoclock experiments, aiming to determine when the electron ionizes from a bound state. The attoclock experiments stimulated renewed efforts towards defining a well-founded tunnel ionization time and determining the tunnel ionization time. A consensus on a suitable definition of tunneling time and the interpretation of experimental results is, however, still lacking [28].

In the case of tunnel ionization the experimental determination of a tunneling time is complicated by the fact that it is notoriously difficult to determine the starting (and ending) moment of the tunnel dynamics. There is no apparent reason to assume that the electron enters the barrier at the instant of the electric field maximum. In fact, we are going to demonstrate that one has to carefully distinguish between the tunneling time, i. e., the time to cross the tunneling barrier, and the tunneling delay, i. e., the time delay until the electron becomes quasi-free with respect to some external reference, e. g., the moment of maximal electric field strength.

Experimentally the quantum dynamics in the vicinity of the tunneling barrier cannot be studied directly, i. e., it is not

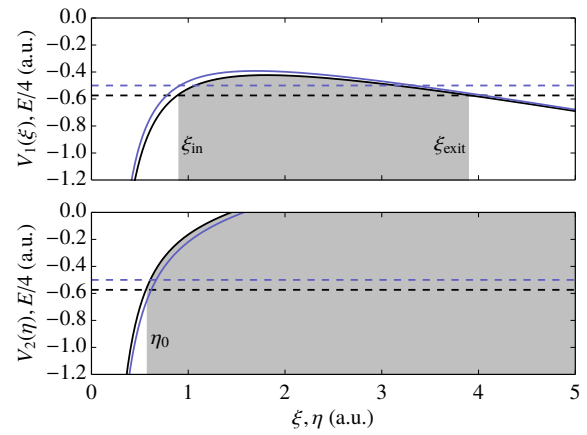


FIG. 1: Tunneling potentials $V_1(\xi)$ and $V_2(\eta)$ (solid lines) and the ground state energy level E (dashed lines) for the two-dimensional Coulomb problem with (black) and without (light blue) accounting for the Stark effect in parabolic coordinates ξ and η for $\mathcal{E} = 1$ a.u. Intersections between the potential lines and the energy level determine the borders between classically allowed classically forbidden regions, i. e., the tunneling entry ξ_{in} , tunneling exit ξ_{exit} , and η_0 . See Appendix for details.

possible to place a detector close to the atomic tunneling barrier. Thus, information about the tunneling dynamics has to be inferred from measurable asymptotic quantities, e. g., the momentum distribution of the photo ionized electrons. In attoclock experiments, an electron is ionized by an elliptically polarized few-cycle pulse. This quasi-free electron is accelerated in the rotating electric field and in this way the instant of ionization t_{exit} is mapped to the final angle of the momentum vector in the polarization plane. Ignoring Coulomb effects as well as non-dipole effects, the electron's final momentum $\mathbf{p}(t_f)$ and the instant of ionization t_{exit} are related according to the two-step model [29–32] via

$$\mathbf{p}(t_f) = \mathbf{p}(t_{\text{exit}}) + q \int_{t_{\text{exit}}}^{t_f} \mathbf{E}(t) dt, \quad (1)$$

where $\mathbf{E}(t)$ denotes the electric field, which vanishes for $t \rightarrow t_f$, q denotes the electron's charge, and $\mathbf{p}(t_{\text{exit}})$ is its initial momen-

^{*} nicolas.teeny@mpi-hd.mpg.de

[†] heiko.bauke@mpi-hd.mpg.de

tum, which is usually assumed to be zero. Assuming that the ionized electron becomes free at the instant of the electric field maximum t_0 , the formula (1) predicts a final momentum with a specific direction [26]. Deviations of an experimentally observed final momentum direction from this prediction may be due to a delay between the instant of maximal field strength and the instant of ionization, i. e., $t_0 \neq t_{\text{exit}}$. But also Coulomb effects [33], a nonzero initial momentum $\mathbf{p}(t_{\text{exit}})$ [27], nondipole effects, or quantum effects, which may play a role for the dynamics at the vicinity of the tunneling exit, cause derivations from the simple two-step model (1). Thus, the interpretation of attoclock experiments requires a precise model of the electron's motion from the barrier exit to the detector. The value of a possible tunneling delay depends crucially on the theoretical model [24], which is employed to calibrate the attoclock.

In view of the difficulties of determining tunneling times from asymptotic momentum measurements, we consider a complementary theoretical approach based on *ab initio* solutions of the time-dependent Schrödinger equation and virtual detectors [34, 35], which allows us to link tunneling times to observables related to the quantum dynamics in the vicinity of the tunneling barrier. This paper is organized as follows: To keep the presentation self-contained, the concept of a virtual detector is summarized in Sec. 2. In Sec. 3 numerical results for tunneling times as determined by the virtual detector approach are presented and discussed. Mainly, we answer the questions: When does the electron enter the barrier and exit the tunneling barrier; and, accordingly, how much time does the electron spend under the barrier? Additionally, we compare the quantum trajectory of the electron to the one predicted by the two-step model [29–32]. Finally, we conclude in Sec. 4.

2. Virtual detectors

2.1. Fundamentals

Ionization from a binding potential means that an electron moves away from the vicinity of the binding potential's minimum. A virtual detector allows to quantify this dynamics. More specifically, a virtual detector is a hypothetical device that determines how the probability to find a particle within some specific space region changes over time. In the following, we lay down its mathematical foundations.

The quantum mechanical evolution of an electron's wave function $\Psi(\mathbf{r}, t)$ with mass m and charge q is governed by the Schrödinger equation

$$i\hbar \frac{\partial \Psi(\mathbf{r}, t)}{\partial t} = \left(\frac{1}{2m} (-i\hbar \nabla - q\mathbf{A}(\mathbf{r}, t))^2 + q\phi(\mathbf{r}, t) \right) \Psi(\mathbf{r}, t), \quad (2)$$

where $\phi(\mathbf{r}, t)$ and $\mathbf{A}(\mathbf{r}, t)$ denote the electromagnetic potentials. The probability density to find the electron at position \mathbf{r} at time t is given by

$$\varrho(\mathbf{r}, t) = \Psi(\mathbf{r}, t)^* \Psi(\mathbf{r}, t), \quad (3)$$

where $\Psi(\mathbf{r}, t)^*$ indicates the complex conjugate of $\Psi(\mathbf{r}, t)$. The dynamics of the density $\varrho(\mathbf{r}, t)$ is associated with the probability current

$$\mathbf{j}(\mathbf{r}, t) = \frac{1}{m} \text{Re} (\Psi(\mathbf{r}, t)^* (-i\hbar \nabla - q\mathbf{A}(\mathbf{r}, t)) \Psi(\mathbf{r}, t)). \quad (4)$$

Expressing the wave function $\Psi(\mathbf{r}, t)$ as

$$\Psi(\mathbf{r}, t) = \sqrt{\varrho(\mathbf{r}, t)} \exp(i\varphi(\mathbf{r}, t)), \quad (5)$$

the probability current $\mathbf{j}(\mathbf{r}, t)$ may be written as a product of the probability density $\varrho(\mathbf{r}, t)$ and some local velocity, viz.

$$\mathbf{j}(\mathbf{r}, t) = \frac{\varrho(\mathbf{r}, t)}{m} (\hbar \nabla \varphi(\mathbf{r}, t) - q\mathbf{A}(\mathbf{r}, t)), \quad (6)$$

which also occurs in the framework of Bohmian mechanics [36]. The probability density and the probability current fulfill the continuity equation

$$-\frac{\partial \varrho(\mathbf{r}, t)}{\partial t} = \nabla \cdot \mathbf{j}(\mathbf{r}, t). \quad (7)$$

For any compact subspace V of the physical space with a piecewise smooth boundary S the continuity equation (7) yields by integration over the subspace

$$-\frac{d}{dt} \int_V \varrho(\mathbf{r}, t) dV = \int_S \mathbf{j}(\mathbf{r}, t) \cdot \mathbf{n} dS, \quad (8)$$

where \mathbf{n} denotes the outward pointing unit normal field of the boundary S . Equation (8) holds also for unbounded subspaces if $\varrho(\mathbf{r}, t)$ decreases fast enough when $|\mathbf{r}| \rightarrow \infty$. Thus, the rate of the change of the probability to find the electron within the space region V is given by the probability current through the volume's surface

$$D_S(t) = \int_S \mathbf{j}(\mathbf{r}, t) \cdot \mathbf{n} dS. \quad (9)$$

A virtual detector is a hypothetical device that measures $D_S(t)$. In other words, a virtual detector placed at the surface S determines how much probability passes from one side of the surface to the other per unit time. Placing S at sufficient distance around a bound wave packet, which is ionized by a time-dependent electric field $\mathbf{E}(t)$ with $\lim_{t \rightarrow \pm\infty} \mathbf{E}(t) = 0$, then $\int_{-\infty}^{\infty} D_S(t) dt$ equals the total ionization probability. Furthermore, if $D_S(t)$ is strictly nonnegative or nonpositive $|D_S(t)|\Delta t$ can be interpreted as the probability that the electron moves from one side of the surface S to the other within the short time interval $[t, t + \Delta t]$.

2.2. Tunnel ionization from a two-dimensional Coulomb potential

In the following, we will study tunnel ionization from a two-dimensional Coulomb potential. The restriction to two dimensions is mainly because this system resembles tunnel ionization from hydrogen-like ions while keeping the computational demands small. In the long-wavelength limit, i. e., when the dipole

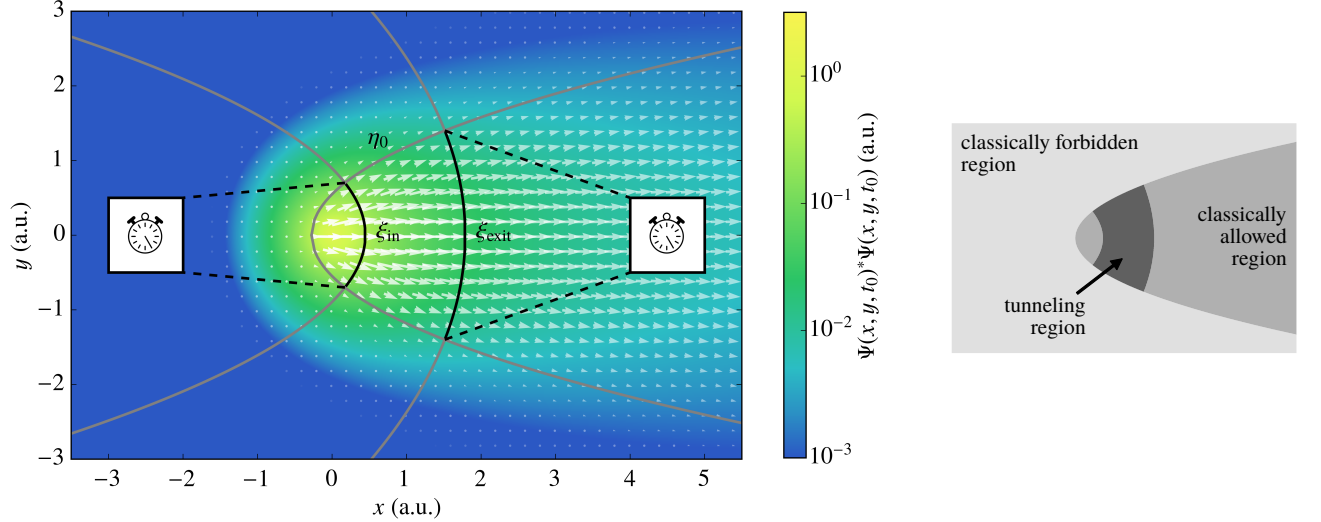


FIG. 2: Schematic of tunneling time determination via virtual detectors at the tunneling entry and the tunneling exit. The lines $\xi = \xi_{in,out}$ and $\eta = \eta_0$ which determine tunneling region, the classically forbidden, and the classical allowed regions are indicated by the solid lines; see Ref. [37] and Appendix for details. The black solid lines indicate the positions of the virtual detectors. The wave-function's probability density $\Psi(x, y, t)^* \Psi(x, y, t)$ at the instant of electric field maximum, i. e., $t = t_0$, is represented by colors for $\mathcal{E}_0 = 1.1$ a.u. and for the Keldysh parameter $\gamma = 0.25$. Arrows indicate the probability current $j(x, y, t)$, where the arrows' length is proportional to the absolute value of the current and the arrows' opacity scales with the wave-function's probability density.

approximation is applicable, the three-dimensional Coulomb potential with an external linearly polarized electric field has rotational symmetry which makes this system effectively two-dimensional. Furthermore, the two-dimensional Coulomb problem is of interest in its own and has been used to model some semiconductor systems [38–40].

Applying the dipole approximation and choosing the coordinate system such that the linearly polarized external electric field $\mathcal{E}(t)$ points into the (negative) x direction, the Schrödinger equation reads in atomic units, which are applied for the remainder of this article,

$$i \frac{\partial \Psi(x, y, t)}{\partial t} = \hat{H} \Psi(x, y, t) = \left(-\frac{1}{2} \frac{\partial^2}{\partial x^2} - \frac{1}{2} \frac{\partial^2}{\partial y^2} - \frac{1}{\sqrt{x^2 + y^2}} - x \mathcal{E}(t) \right) \Psi(x, y, t). \quad (10)$$

In order to study the ionization dynamics without undesirable artifacts, i. e., to avoid multiple ionization and rescattering, we choose an electric field pulse with a unique maximum,

$$\mathcal{E}(t) = \mathcal{E}_0 \exp\left(-\frac{\omega^2(t - t_0)^2}{2}\right), \quad (11)$$

where t_0 denotes the instant of maximal electric field $\mathcal{E}(t_0) = \mathcal{E}_0$ and $\tau_{\mathcal{E}} = \sqrt{2}/\omega$ is the time scale of the raise and decay of the electric field.

Cartesian coordinates are not the most suitable choice to deal with the Coulomb problem with an external homogeneous electric field. Parabolic coordinates are the natural coordinate system for this problem. In particular, it allows to define a tunneling barrier [41]. As one can show, the Hamiltonian \hat{H} in Eq. (10) separates in parabolic coordinates $0 \leq \xi < \infty$ and

$0 \leq \eta < \infty$, which are related to the Cartesian coordinates x and y via

$$x = \frac{\xi - \eta}{2}, \quad (12a)$$

$$y = \sqrt{\xi \eta}, \quad (12b)$$

into two independent one-dimensional Schrödinger-type Hamiltonians with specific potentials $V_1(\xi)$ and $V_2(\eta)$. While $V_2(\eta)$ is purely attractive, $V_1(\xi)$ represents the tunneling barrier and, therefore, ξ denotes the tunneling direction. Intersections of the potentials with the energy value $E/4$ of the one-dimensional Hamiltonians define the borders between the classically allowed, the tunneling, and the classically forbidden regions. Here, E denotes the Stark-effect corrected ground state energy of the two-dimensional system. The classically allowed, the tunneling, and the classically forbidden regions are characterized by

$$E/4 > V_1(\xi), \quad E/4 > V_2(\eta), \quad (13a)$$

$$E/4 > V_1(\xi), \quad E/4 < V_2(\eta), \quad (13b)$$

$$E/4 < V_1(\xi), \quad E/4 < V_2(\eta), \quad (13c)$$

respectively. The tunneling barrier is confined by the three parabolas at $\xi = \xi_{in}$, $\xi = \xi_{exit}$, and $\eta = \eta_0$, which are functions of the applied electric field strength $\mathcal{E}(t)$. See Appendix for details and also Figs. 1 and 2.

The virtual detectors are placed at $\xi = \xi_{in}$ and $\xi = \xi_{exit}$ as given for the maximal electric field strength \mathcal{E}_0 at $t = t_0$. In two dimensions, the surface integral in Eq. (8) becomes a line integral of a vector field $j(x, y, t)$. Thus, the probability current over the entry line $\xi = \xi_{in}$, denoted by $D_{\xi_{in}}(t)$, and the

current over the exit line $\xi = \xi_{\text{exit}}$, denoted by $D_{\xi_{\text{exit}}}(t)$, are given explicitly by

$$D_{\xi}(t) = \int_0^{\eta_0} j(x(\xi, \eta), y(\xi, \eta), t) \cdot \left(\frac{\partial x(\xi, \eta)}{\partial \eta} \right) d\eta + \int_0^{\eta_0} j(x(\xi, \eta), -y(\xi, \eta), t) \cdot \left(-\frac{\partial y(\xi, \eta)}{\partial \eta} \right) d\eta, \quad (14)$$

where we have taken into account that Eq. (12) covers only the upper half of the coordinate system. Monitoring the probability current at these *fixed* entry and exit lines can be justified as follows. For static fields the tunneling probability is maximal for maximal electric fields and it is exponentially suppressed for lower fields. Furthermore, the applied electric field (11) is quasistatic for $|t - t_0| < \tau_E$, i. e.,

$$\mathcal{E}(t) = \mathcal{E}_0 \left(1 - (t - t_0)^2 / \tau_E^2 + O((t - t_0)^4 / \tau_E^4) \right). \quad (15)$$

Therefore, the tunneling barrier is also quasistatic if times close to t_0 are considered. As it will be shown later, the extracted tunneling times are short compared to τ_E indeed.

3. Numerical results and discussion

3.1. Entry time, exit time, and tunneling time

The Schrödinger equation (10) is solved numerically by employing a Lanczos propagator [42, 43] and fourth-order finite differences for the discretization of the Schrödinger Hamiltonian. The ground state of the two-dimensional Coulomb potential was chosen as an initial condition at $t - t_0 = -5\tau_E$, i. e., when the external electric field is negligible small. The so-called Keldysh parameter $\gamma = \omega \sqrt{-2E_0}/\mathcal{E}_0$ [10] characterizes the ionization process as dominated by tunneling for $\gamma \ll 1$ and by multiphoton ionization for $\gamma \gg 1$. Here, E_0 denotes the ground state binding energy, which equals $E_0 = -2$ a.u. for the two-dimensional Coulomb problem, see also the Appendix. In the following, the electric field amplitude \mathcal{E}_0 and the frequency ω are adjusted such that $\gamma = 0.25 < 1$.

Figure 2 illustrates the ionization dynamics in the vicinity of the tunneling barrier by presenting the electron's probability density $\Psi(x, y, t)^* \Psi(x, y, t)$ and the probability current $j(x, y, t)$ at the instant of maximal field strength $t = t_0$. The external electric field induces a probability current opposite to the direction of the electric field. This flow is nonnegligible only in the region $\eta < \eta_0$, i. e., in the classically allowed region and the tunneling region. Thus, the shape of the probability current confirms that parabolic coordinates are the natural choice to define a tunneling barrier for the Coulomb problem.

The action of the external electric field induces a probability current, which flows over the tunneling barrier's entry line $\xi = \xi_{\text{in}}$ and its exit line $\xi = \xi_{\text{exit}}$. This means, probability is carried over from the center region of the Coulomb potential into the tunneling barrier, from where it can escape into the

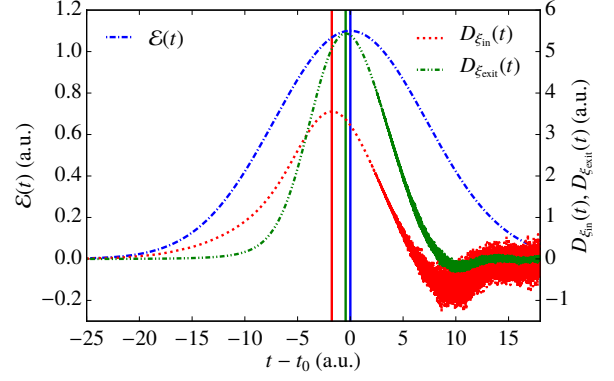


FIG. 3: The probability current $D_{\xi_{\text{in}}}(t)$ over the entry line $\xi = \xi_{\text{in}}$ and the current over $D_{\xi_{\text{exit}}}(t)$ the exit line $\xi = \xi_{\text{exit}}$ and the amplitude of the external electric field $\mathcal{E}(t)$ as functions of time t . The three vertical lines indicate from left to right the moments of maximal probability current over the line $\xi = \xi_{\text{in}}$, of maximal electric field, and of maximal probability current over the line $\xi = \xi_{\text{exit}}$. The parameters of the electric field correspond to a maximal field strengths of $\mathcal{E}_0 = 1.1$ a.u. and a Keldysh parameter $\gamma = 0.25$.

classically allowed region. The quantities $D_{\xi_{\text{in}}}(t)$ and $D_{\xi_{\text{exit}}}(t)$ grow and decay over time with the applied external electric field, as shown in Fig. 3. As a central result of our numerical solution of the Schrödinger equation, however, the position of the maxima of $D_{\xi_{\text{in}}}(t)$, $D_{\xi_{\text{exit}}}(t)$, and the electric field $\mathcal{E}(t)$ do not coincide. The probability current over the tunneling entry $D_{\xi_{\text{in}}}(t)$ reaches its maximum before the maximum of the electric field is attained. Furthermore, the probability current over the tunneling exit $D_{\xi_{\text{exit}}}(t)$ may reach its maximum before or after the maximum of the electric field is attained depending on the electric field strength \mathcal{E}_0 . For the rather strong electric field of the parameters of Fig. 3, $D_{\xi_{\text{exit}}}(t)$ reaches its maximum slightly before the electric field. Turning off the external electric field, the flow at the tunneling entry becomes negative and then oscillates rapidly around zero after switching off the electric field. These oscillations are a result of the excitation of the bound portion of the wave function during the action of the electric field. The final bound state is a superposition of several eigenstates causing a nonsteady probability current. In contrast, the quantity $D_{\xi_{\text{exit}}}(t)$ remains positive as reflections are absent at the tunneling exit and behind the tunneling barrier [27].

Monitoring the probability current at $\xi = \xi_{\text{in}}$ and $\xi = \xi_{\text{exit}}$ allows us to determine the moments when the electrons enters or leaves the tunneling barrier with maximal probability. The probability to cross the tunneling barrier entry at $\xi = \xi_{\text{in}}$ or the exit at $\xi = \xi_{\text{exit}}$ during the small time interval $[t, t + \Delta t]$ is $\Delta t D_{\xi_{\text{in}}}(t)$ and $\Delta t D_{\xi_{\text{exit}}}(t)$, respectively. This motivates us to introduce the times of maximal flow over the tunneling entry and exit as

$$t_{\text{in}} = \arg \max D_{\xi_{\text{in}}}(t) \quad (16)$$

and

$$t_{\text{exit}} = \arg \max D_{\xi_{\text{exit}}}(t). \quad (17)$$

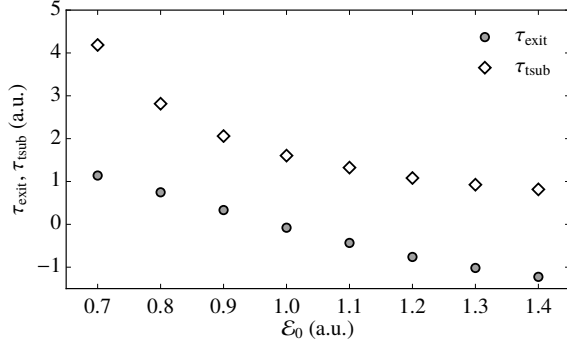


FIG. 4: The tunneling delay τ_{sub} and the tunneling time τ_{exit} as functions of the electric field amplitude \mathcal{E}_0 . The frequency ω is adjusted such that the Keldysh parameter is fixed to $\gamma = 0.25$.

Then the delay between the instant of the maximum of the driving electric field t_0 and the exit time t_{exit} , the tunneling delay, is

$$\tau_{\text{exit}} = t_{\text{exit}} - t_0 \quad (18)$$

and the tunneling time

$$\tau_{\text{sub}} = t_{\text{exit}} - t_{\text{in}} \quad (19)$$

can be introduced with the definitions above. A measurement of the delay τ_{exit} is implemented in the attoclock experiments. The time τ_{sub} denotes the delay between the instants when the probability flow is maximal at the tunneling-barrier's entry and at the exit. Thus, τ_{sub} may be interpreted as the typical time which an electron needs to pass the tunneling barrier.

The times τ_{exit} and τ_{sub} are presented in Fig. 4 for the considered setup and varying electric field amplitudes \mathcal{E}_0 . An increasing electric field amplitude reduces the width of the tunneling barrier. Consequently, the tunneling time τ_{sub} decreases with increasing electric field amplitude \mathcal{E}_0 , as shown in Fig. 4. The time τ_{sub} remains, however, always positive. This means, the probability current reaches its maximum at the entry of the tunneling barrier before the current becomes maximal at the exit, i. e., the electron enters the barrier before it exits the barrier. Furthermore, it follows from the data in Fig. 4 that $\tau_{\text{sub}} > \tau_{\text{exit}}$ and consequently $t_{\text{entry}} < t_0$, because $\tau_{\text{sub}} - \tau_{\text{exit}} = t_0 - t_{\text{entry}}$. This means, the electron always enters the tunneling barrier before the electric field reaches its maximum.

To explain the reason for this behavior, we define in analogy to Eq. (14) the two integrals over the probability density

$$D_{\xi}^{\rho}(t) = \int_0^{\eta_0} \varrho(x(\xi, \eta), y(\xi, \eta), t) d\eta + \int_0^{\eta_0} \varrho(x(\xi, \eta), -y(\xi, \eta), t) d\eta \quad (20)$$

and over the velocity field

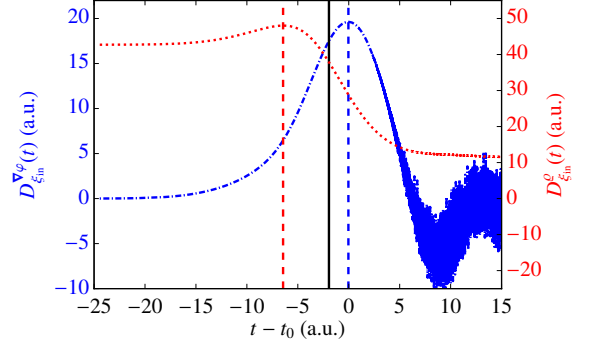


FIG. 5: The probability density $D_{\xi_{\text{in}}}^{\rho}(t)$ (red dashed line, right scale) and the local velocity $D_{\xi_{\text{in}}}^{\nabla\varphi}(t)$ (blue dot-dashed line, left scale) along the entry line $\xi = \xi_{\text{in}}$ are plotted in function of time for the electric field strength $\mathcal{E}_0 = 1.3$ a.u. The solid black line denotes the instant of maximal $D_{\xi_{\text{in}}}^{\rho}(t)$, vertical dashed lines indicate the position of the maxima of $D_{\xi_{\text{in}}}^{\rho}(t)$ and $D_{\xi_{\text{in}}}^{\nabla\varphi}(t)$.

$$D_{\xi}^{\nabla\varphi}(t) = \int_0^{\eta_0} \nabla\varphi(x(\xi, \eta), y(\xi, \eta), t) \cdot \begin{pmatrix} \frac{\partial x(\xi, \eta)}{\partial \eta} \\ \frac{\partial y(\xi, \eta)}{\partial \eta} \end{pmatrix} d\eta + \int_0^{\eta_0} \nabla\varphi(x(\xi, \eta), -y(\xi, \eta), t) \cdot \begin{pmatrix} \frac{\partial x(\xi, \eta)}{\partial \eta} \\ -\frac{\partial y(\xi, \eta)}{\partial \eta} \end{pmatrix} d\eta, \quad (21)$$

which are motivated by fact that the probability current can be written as a product of the probability density and the local velocity, see Eq. (6). $D_{\xi_{\text{in}}}^{\rho}(t)$ gives the probability density integrated along the entry line $\xi = \xi_{\text{in}}$ in function of time, while $D_{\xi_{\text{in}}}^{\nabla\varphi}(t)$ denotes the integrated velocity. As shown in Fig. 5, the velocity along the entry line $D_{\xi_{\text{in}}}^{\nabla\varphi}(t)$ increases with the electric field, reaches a maximum at the instant of electric field maximum $t = t_0$, then decreases with the electric field and it becomes even negative due to reflections from the tunneling process. Finally, the integrated velocity $D_{\xi_{\text{in}}}^{\nabla\varphi}(t)$ oscillates around zero indicating the excitation of the bound state. The probability density along the entry line $D_{\xi_{\text{in}}}^{\rho}(t)$ is nonzero even at $t \ll t_0$ because the wave function penetrates tunneling barrier even for $\mathcal{E} = 0$. Increasing the electric field, the probability density flow from the core into the barrier increases the probability density along the entry line. Although the local velocity at the tunneling entry is maximal at $t = t_0$ in sync with the electric field, the probability flow along the entry line $D_{\xi_{\text{in}}}^{\rho}(t)$ reaches its maximum earlier. The quantity $D_{\xi_{\text{in}}}^{\rho}(t)$ goes asymptotically to a constant value less than the initial value because some of the total probability has tunneled. Because the probability flow is the product of the probability density and the local velocity, the maximum of the integrated probability flow $D_{\xi_{\text{in}}}^{\rho}(t)$ is reached between the instants of the maxima of the integrated density $D_{\xi_{\text{in}}}^{\rho}(t)$ and the integrated velocity $D_{\xi_{\text{in}}}^{\nabla\varphi}(t)$, this means $t_{\text{in}} < t_0$. The time t_{exit} is usually larger than t_0 , i. e., $\tau_{\text{exit}} > 0$, especially for weak external fields.

After the electron has passed the entry line of the tunneling barrier, it needs some time to cross the barrier and to reach

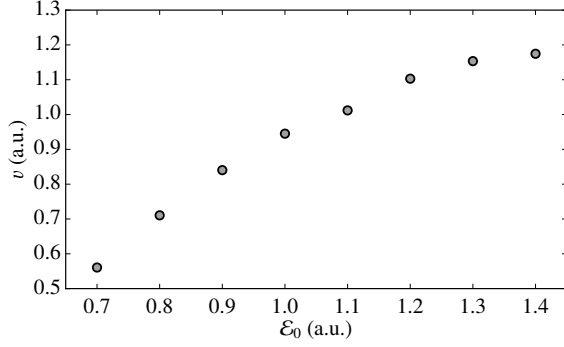


FIG. 6: Average velocity v of the motion of the probability-current's maximum from the tunneling barrier entry to the exit as a function of the applied maximal electric field strength \mathcal{E}_0 .

the tunneling exit. This means, $t_{\text{exit}} > t_{\text{in}}$, but not necessarily $t_{\text{exit}} > t_0$. The latter may be understood by realizing that the above explanation for $t_{\text{in}} < t_0$ is not specific to the coordinate $\xi = \xi_{\text{in}}$. In particular, it also applies to $\xi = \xi_{\text{exit}}$. Consequently, also the integrated flow at the exit coordinate $D_{\xi_{\text{exit}}}^{\rho}(t)$ may reach its maximum before the maximum of the electric field, as for example for the parameters in Fig. 3. In general, however, we find that $D_{\xi_{\text{exit}}}^{\nabla\varphi}(t)$ is maximal at an instant very close to t_0 .

Taking the results above into consideration, the time t_{in} should be regarded as a reference for the tunneling time, but not t_0 which leads to the delay τ_{exit} . Choosing t_0 as a reference can lead to negative delays τ_{exit} for large electric field strengths, e. g., for $\mathcal{E}_0 \geq 1.0$ a.u. for the setup that was applied for Fig. 4. This, however, should not be misinterpreted as a negative tunneling time because τ_{exit} is not related to the time which an electron needs to pass the tunneling barrier. This time is given by τ_{tsub} . As τ_{tsub} is always larger than τ_{exit} , the delay τ_{exit} may be used as a lower bound of the tunneling time.

It has been speculated that tunnel ionization may be instantaneous [13, 24], which would be associated with a superluminal traversal of the tunneling barrier. Our results, however, clearly indicate that there is a nonvanishing tunneling time τ_{tsub} . This leads to a finite average velocity of the motion of from $\xi = \xi_{\text{in}}$ to $\xi = \xi_{\text{exit}}$

$$v = \frac{\xi_{\text{exit}} - \xi_{\text{in}}}{2\tau_{\text{tsub}}}. \quad (22)$$

Here we have taken into account that the lines of constant ξ are parabolas in the x - y plane and the probability current flows mainly at $y \approx 0$. As shown in Fig. 6, there is a monotonous relation between the applied maximal electric field strength \mathcal{E}_0 and the velocity v . The velocity presented in Fig. 6, however, is more than two orders of magnitude below the speed of light. Identifying the tunneling motion of the electron over the tunneling barrier with the motion of the probability-current's maximum, it is justified to say that tunneling ionization is neither instantaneous nor moves the electron at superluminal speed.

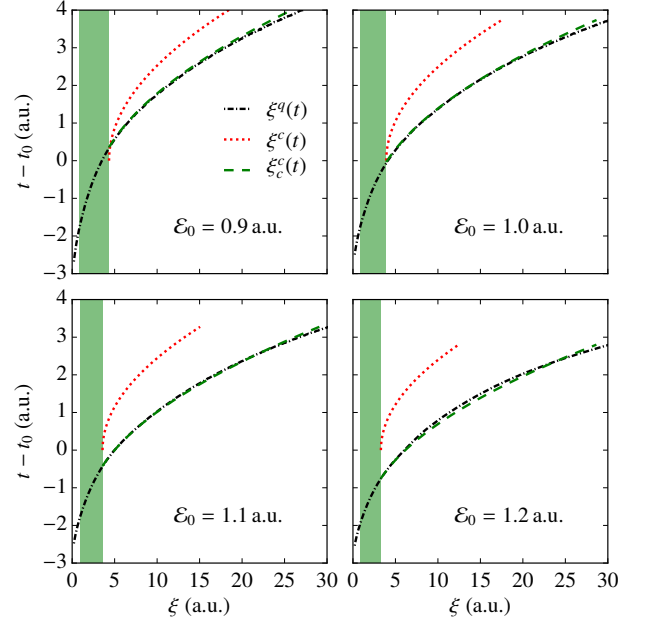


FIG. 7: The quantum trajectory of the electron in the ξ coordinate $\xi^q(t)$, compared to the classical trajectory according based on the two-step model $\xi^c(t)$. Both are also compared to the classical trajectory corrected according to quantum initial conditions $\xi^c_c(t)$. For more information see text. The shadowed area marks the positions ξ corresponding to under the barrier.

3.2. Quantum and classical trajectories

The probability currents over different lines of constant ξ reaches their maxima at different times, which allows us to define a quantum trajectory $\xi^q(t)$ by inverting

$$t_{\xi} = \arg \max D_{\xi}(t). \quad (23)$$

The quantum trajectory $\xi^q(t)$ defined by Eq. (23) can be compared to the trajectory predicted by a Coulomb corrected two-step model $\xi^c(t)$. This classical trajectory is determined by the Newton equation

$$\frac{d^2 \xi^c(t)}{dt^2} = -\frac{8}{\xi^c(t)^2} + 2\mathcal{E}(t), \quad (24)$$

where the reduction to one dimension is justified as the most probable trajectory is along the x direction at $y \approx 0$. The initial conditions for the two-step model are

$$\xi^c(t_0) = \xi_{\text{exit}}, \quad (25a)$$

$$\left. \frac{d\xi^c(t)}{dt} \right|_{t=t_0} = 0 \quad (25b)$$

meaning that the electron exits at the instant of electric field maximum $t = t_0$ with zero initial momentum at the turning point $x = \xi_{\text{exit}}/2$. As shown in Fig. 7 for different electric field strengths, the classical trajectory $\xi^c(t)$ deviates from the quantum trajectory $\xi^q(t)$ not only near the barrier exit but also at a far away detector, i. e., for $\xi \gg \xi_{\text{exit}}$.

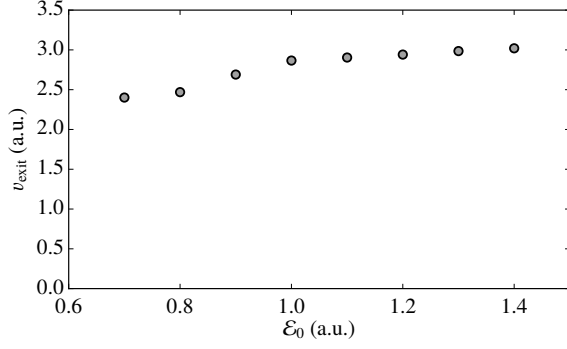


FIG. 8: The quantum trajectory's initial velocity v_{exit} plotted for different electric field strengths E_0 for Keldysh parameter $\gamma = 0.25$.

From the above studies we have seen that the electron exits the tunneling barrier at t_{exit} , which differs from t_0 . It has been shown by quantum mechanical calculations [27] that the electron exits also with an initial momentum in the electric field direction. This initial velocity can be inferred from the quantum trajectory, via

$$v_{\text{exit}} = \left. \frac{d\xi^q(t)}{dt} \right|_{t=t_{\text{exit}}}, \quad (26)$$

which yields results that are consistent with the results of Ref. [27]. The classical trajectory $\xi^c(t)$ can be corrected by the quantum initial conditions

$$\xi_c^c(t_{\text{exit}}) = \xi_{\text{exit}}, \quad (27a)$$

$$\left. \frac{d\xi_c^c(t)}{dt} \right|_{t=t_{\text{exit}}} = v_{\text{exit}}. \quad (27b)$$

As shown in Fig. 7 the corrected classical trajectory $\xi_c^c(t)$ agrees well with the quantum trajectory $\xi^q(t)$. Nevertheless, there is still a slight discrepancy between both trajectories at a far away detector, which can be attributed to that $\xi^q(t)$ originates from the motion of a broad wave packet which experiences a spatially varying Coulomb force [44]. The initial velocity v_{exit} is plotted in Fig. 8 for different electric field strengths. In agreement with [27], the initial momentum is slightly dependent on the electric field strength also in the considered two-dimensional system. The initial momentum is of the order of width of the ground state distribution in momentum space.

The initial velocity v_{exit} is difficult to measure directly in an experiment. But it also affects the asymptotic velocity of the ionized electron. Note that one can choose an electric field strength such that the quantum trajectory is at $\xi^q = \xi_{\text{exit}}$ at $t = t_0$, i. e., the electron leaves the tunneling barrier at the moment of electric-field maximum, which is one assumption of the two-step model. In this case, the difference between the electron's actual asymptotic momentum and the prediction of the classical Coulomb-corrected two-step model is just the electron's initial momentum at the barrier exit. For the two-dimensional model as considered in Fig. 7 the condition $\xi^q(t_0) = \xi_{\text{exit}}$ is fulfilled for an electric field strength $E_0 = 1.0$ a.u.

4. Conclusions

We studied the dynamics of tunnel ionization by analyzing the quantum mechanical wave-function's probability current via virtual detectors. Virtual detectors are a capable concept for determining tunneling times because they allow to identify well-defined moments when the ionized electron enters and leaves the tunneling barrier.

The numerical solutions of the time-dependent Schrödinger equation and the dynamics of the probability current at the tunneling barrier indicate that the electron spends a nonvanishing time under the potential barrier. This corresponds to a crossing velocity that is much lower than the speed of light. Furthermore, the electron may enter the classical forbidden region on average before the instant of the maximum of the driving electric field. Therefore, the instant of electric field maximum should not be considered as an initial reference time of the tunneling process. Nevertheless, for electric field strengths well below the threshold regime the electron exits the barrier after the instant of electric field maximum. For such strengths a nonvanishing delay τ_{exit} between the electric field maximum and the emergence of the electron behind the tunneling barrier exists as a signature of the time spent under the barrier. The actual time span that the electron has spent in the classically forbidden region, however, will be larger than τ_{exit} . Vanishing or negative time delays τ_{exit} should not be interpreted as instantaneous tunneling.

Under the barrier as well at the tunneling exit, the electron has a nonzero velocity in electric field direction. After the tunneling exit, the quantum trajectory, which is induced by the wave-function's probability current, agrees well with a trajectory as given by classical equations of motion when the electron's initial velocity at the tunneling exit is taken into account properly.

Acknowledgments

We gratefully thank Enderalp Yakaboylu for valuable discussions.

A. The Coulomb problem and the Strak effect in two dimensions

The eigen equation of the two-dimensional Coulomb problem [39, 45] with some additional homogeneous electric field of strength \mathcal{E} is given in Cartesian coordinates x and y and employing atomic units by

$$\left(-\frac{1}{2} \frac{\partial^2}{\partial x^2} - \frac{1}{2} \frac{\partial^2}{\partial y^2} - \frac{1}{\sqrt{x^2 + y^2}} - \mathcal{E}x \right) \Psi(x, y) = E \Psi(x, y), \quad (A.1)$$

where $\Psi(x, y)$ denotes an eigen function with energy E . This eigen equation separates in parabolic coordinates ξ and η [45–47], which are related to the Cartesian coordinates x and y

via Eq. (12). This coordinate system is particularly useful because here the two-dimensional Schrödinger equation can be separated into two one-dimensional Schrödinger equations, which allows to define a one-dimensional tunneling barrier. The calculations in this section follow Ref. [48], where the three-dimensional Coulomb problem is considered in a similar way.

The Laplacian becomes in the new coordinate system

$$\frac{\partial^2}{\partial x^2} + \frac{\partial^2}{\partial y^2} = \frac{1}{\xi + \eta} \left(4\xi \frac{\partial^2}{\partial \xi^2} + 2 \frac{\partial}{\partial \xi} + 4\eta \frac{\partial^2}{\partial \eta^2} + 2 \frac{\partial}{\partial \eta} \right). \quad (\text{A.2})$$

Expressing (A.1) in parabolic coordinates yields after some algebraic transformations

$$\begin{aligned} & \left(\xi \frac{\partial^2}{\partial \xi^2} + \frac{1}{2} \frac{\partial}{\partial \xi} + \frac{E}{2} \xi + \frac{\mathcal{E}}{4} \xi^2 \right) \Psi(\xi, \eta) + \\ & \left(\eta \frac{\partial^2}{\partial \eta^2} + \frac{1}{2} \frac{\partial}{\partial \eta} + \frac{E}{2} \eta - \frac{\mathcal{E}}{4} \eta^2 \right) \Psi(\xi, \eta) = -\Psi(\xi, \eta). \end{aligned} \quad (\text{A.3})$$

Substituting the ansatz $\Psi(\xi, \eta) = f_1(\xi)f_2(\eta)$ into the last equation and separating the variables ξ and η we obtain the two equations

$$\left(\xi \frac{\partial^2}{\partial \xi^2} + \frac{1}{2} \frac{\partial}{\partial \xi} + \frac{E}{2} \xi + \frac{\mathcal{E}}{4} \xi^2 + \beta_1 \right) f_1(\xi) = 0, \quad (\text{A.4a})$$

$$\left(\eta \frac{\partial^2}{\partial \eta^2} + \frac{1}{2} \frac{\partial}{\partial \eta} + \frac{E}{2} \eta - \frac{\mathcal{E}}{4} \eta^2 + \beta_2 \right) f_2(\eta) = 0, \quad (\text{A.4b})$$

where the separation constants β_1 and β_2 are related by

$$\beta_1 + \beta_2 = 1. \quad (\text{A.5})$$

The tunneling barriers are obtained by substituting $f_1(\xi) = g_1(\xi)/\xi^{1/4}$ and $f_2(\eta) = g_2(\eta)/\eta^{1/4}$, which gives the equations for the new functions as

$$-\frac{1}{2} \frac{\partial^2 g_1(\xi)}{\partial \xi^2} + \left(-\frac{3}{32\xi^2} - \frac{\beta_1}{2\xi} - \frac{\xi}{8}\mathcal{E} \right) g_1(\xi) = \frac{E}{4} g_1(\xi), \quad (\text{A.6a})$$

$$-\frac{1}{2} \frac{\partial^2 g_2(\eta)}{\partial \eta^2} + \left(-\frac{3}{32\eta^2} - \frac{\beta_2}{2\eta} + \frac{\eta}{8}\mathcal{E} \right) g_2(\eta) = \frac{E}{4} g_2(\eta). \quad (\text{A.6b})$$

These two equations represent Schrödinger-type eigen equations with potentials

$$V_1(\xi) = -\frac{3}{32\xi^2} - \frac{\beta_1}{2\xi} - \frac{\xi}{8}\mathcal{E}, \quad (\text{A.7a})$$

$$V_2(\eta) = -\frac{3}{32\eta^2} - \frac{\beta_2}{2\eta} + \frac{\eta}{8}\mathcal{E} \quad (\text{A.7b})$$

and the energy $E/4$.

For a vanishing external electric field, i.e., $\mathcal{E} = 0$, Eqs. (A.4a) and (A.4b) are identical. Introducing the variable transformation $\xi = \eta = \zeta/\sqrt{-2E}$ gives in this case

$$\left(\zeta \frac{\partial^2}{\partial \zeta^2} + \frac{1}{2} \frac{\partial}{\partial \zeta} + \frac{\beta_{1,2}}{\sqrt{-2E}} - \frac{\zeta}{4} \right) f_{1,2}(\zeta) = 0. \quad (\text{A.8})$$

Making the ansatz $f_{1,2}(\zeta) = \exp(-\zeta/2)g_{1,2}(\zeta)$ this differential equation yields the equation

$$\left(\zeta \frac{\partial^2}{\partial \zeta^2} + \left(\frac{1}{2} - \zeta \right) \frac{\partial}{\partial \zeta} - \left(\frac{1}{4} - \frac{\beta_{1,2}}{\sqrt{-2E}} \right) \right) g_{1,2}(\zeta) = 0 \quad (\text{A.9})$$

for $g_{1,2}(\zeta)$, which can be identified as the confluent hypergeometric equation [49] with

$$a = \frac{1}{4} - \frac{\beta_{1,2}}{\sqrt{-2E}}, \quad b = \frac{1}{2}. \quad (\text{A.10})$$

The nonsingular solution of the confluent hypergeometric equation is usually called confluent hypergeometric function and denoted by ${}_1F_1(a; b; \zeta)$ or $M(a; b; \zeta)$. Thus we have found the solution

$$f_1(\xi) \sim \exp\left(-\frac{\xi}{2}\sqrt{-2E}\right) M\left(\frac{1}{4} - \frac{\beta_1}{\sqrt{-2E}}; \frac{1}{2}; \xi\sqrt{-2E}\right) \quad (\text{A.11})$$

and similar for $f_2(\eta)$. These functions $f_1(\xi)$ and $f_2(\eta)$ can be normalized only if the first argument of the confluent hypergeometric function is a negative integer or zero. In this case the confluent hypergeometric function coincides (up to normalization) with the associated Laguerre polynomials. Thus, the quantization conditions

$$\frac{1}{4} - \frac{\beta_{1,2}}{\sqrt{-2E}} = -n_{1,2} \quad (\text{A.12})$$

with $n_{1,2} = 0, 1, 2, \dots$ with have to be fulfilled. Together with the relation (A.5) the quantization conditions yield

$$E = -\frac{1}{2(n_1 + n_2 + 1/2)^2}, \quad (\text{A.13})$$

$$\beta_{1,2} = \left(n_{1,2} + \frac{1}{4} \right) \sqrt{-2E}. \quad (\text{A.14})$$

Normalizing $f_1(\xi)$ and $f_2(\eta)$ to unity finally gives the bound eigen states of the two-dimensional Coulomb problem $\Psi_{n_1, n_2}(\xi, \eta) = f_{1;E, n_1}(\xi)f_{2;E, n_2}(\eta)$ with

$$f_{1;E, n_1}(\xi) = \sqrt{\frac{\sqrt{-2E}}{1 + 4n_1}} \exp\left(-\frac{\xi}{2}\sqrt{-2E}\right) M\left(-n_1; \frac{1}{2}; \xi\sqrt{-2E}\right), \quad (\text{A.15a})$$

$$f_{2;E, n_2}(\eta) = \sqrt{\frac{\sqrt{-2E}}{1 + 4n_2}} \exp\left(-\frac{\eta}{2}\sqrt{-2E}\right) M\left(-n_2; \frac{1}{2}; \eta\sqrt{-2E}\right) \quad (\text{A.15b})$$

and the energy E given by (A.13).

Taking into account the Stark effect, i.e., $\mathcal{E} > 0$, leads to a modification of the eigen states, of the eigen energies E , as well as of the separation constants β_1 and β_2 . In this way, also the tunneling potential (A.7a) changes. The resulting values for β_1, β_2 , and E can be calculated via perturbation theory [48]. In case of the ground state with $n_1 = n_2 = 0$, we get in second order

$$\beta_{1,2} = \beta_{1,2}^{(0)} + \beta_{1,2}^{(1)} + \beta_{1,2}^{(2)} \quad (\text{A.16})$$

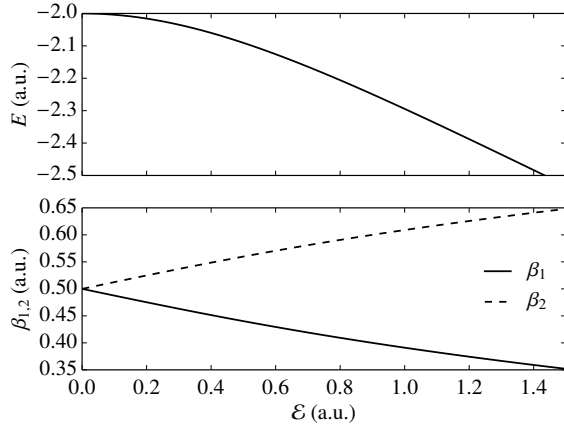


FIG. 9: The ground state energy E of the two-dimensional Coulomb problem with an external electric field and the separation parameters β_1 and β_2 as functions of the electric field strength \mathcal{E} .

with

$$\beta_{1,2}^{(0)} = \sqrt{-E/8}, \quad (\text{A.17a})$$

$$\beta_{1,2}^{(1)} = \int f_{1,2;E,0}(\xi) \left(\mp \frac{\xi}{4} \mathcal{E} \right) f_{1,2;E,0}(\xi) d\xi = \mp \frac{\mathcal{E}}{4E}, \quad (\text{A.17b})$$

$$\begin{aligned} \beta_{1,2}^{(2)} &= \frac{1}{\sqrt{-2E}} \times \\ &\sum_{n=1}^{\infty} \frac{1}{\frac{1}{4} - (n + \frac{1}{4})} \left| \int f_{1,2;E,n}(\xi) \left(\mp \frac{\xi}{4} \mathcal{E} \right) f_{1,2;E,0}(\xi) d\xi \right|^2 \\ &\approx 0.2004642410 \sqrt{-2E} \frac{\mathcal{E}^2}{E^3}. \end{aligned} \quad (\text{A.17c})$$

The Eqs. (A.16) and (A.5) determine the parameters β_1 , β_2 , and E uniquely and the results of a numerical solution of these equations is shown in Fig. 9.

-
- [1] L. A. MacColl, “Note on the transmission and reflection of wave packets by potential barriers,” *Phys. Rev.* **40**, 621–626 (1932).
 - [2] E. H. Hauge and J. A. Støvneng, “Tunneling times: a critical review,” *Rev. Mod. Phys.* **61**, 917–936 (1989).
 - [3] R. Landauer and Th. Martin, “Barrier interaction time in tunneling,” *Rev. Mod. Phys.* **66**, 217–228 (1994).
 - [4] Kaushik Maji, C. K. Mondal, and S. P. Bhattacharyya, “Tunneling time and tunnelling dynamics,” *Int. Rev. Phys. Chem.* **26**, 647–670 (2007).
 - [5] A. M. Steinberg, P. G. Kwiat, and R. Y. Chiao, “Measurement of the single-photon tunneling time,” *Phys. Rev. Lett.* **71**, 708–711 (1993).
 - [6] P. Guéret, E. Marclay, and H. Meier, “Experimental observation of the dynamical image potential in extremely low GaAs/Al_xGa_{1-x}As/GaAs tunnel barriers,” *Appl. Phys. Lett.* **53**, 1617–1619 (1988).
 - [7] D. Mugnai, A. Ranfagni, and R. Ruggeri, “Observation of superluminal behaviors in wave propagation,” *Phys. Rev. Lett.* **84**, 4830–4833 (2000).
 - [8] A. Enders and G. Nimtz, “Evanescent-mode propagation and quantum tunneling,” *Phys. Rev. E* **48**, 632–634 (1993).
 - [9] Herbert G. Winful, “Tunneling time, the Hartman effect, and superluminality: A proposed resolution of an old paradox,” *Phys. Rep.* **436**, 1–69 (2006).
 - [10] L. V. Keldysh, “Ionization in the field of a strong electromagnetic wave,” *Sov. Phys.-JETP* **20**, 1307–1314 (1965).
 - [11] M. Uiberacker, Th. Uphues, M. Schultze, A. J. Verhoef, V. Yakovlev, M. F. Kling, J. Rauschenberger, N. M. Kabachnik, H. Schröder, M. Lezius, K. L. Kompa, H.-G. Muller, M. J. J. Vrakking, S. Hendel, U. Kleineberg, U. Heinzmann, M. Drescher, and F. Krausz, “Attosecond real-time observation of electron tunnelling in atoms,” *Nature* **446**, 627–632 (2007).
 - [12] Yue Ban, E. Ya. Sherman, J. G. Muga, and M. Büttiker, “Time scales of tunneling decay of a localized state,” *Phys. Rev. A* **82**, 062121 (2010).
 - [13] P. Eckle, A. N. Pfeiffer, C. Cirelli, A. Staudte, R. Dörner, H. G. Muller, M. Büttiker, and U. Keller, “Attosecond ionization and tunneling delay time measurements in helium,” *Science* **322**, 1525–1529 (2008).
 - [14] Petrisa Eckle, Mathias Smolarski, Philip Schlup, Jens Biegert, André Staudte, Markus Schöffler, Harm G. Muller, Reinhard Dörner, and Ursula Keller, “Attosecond angular streaking,” *Nat. Phys.* **4**, 565–570 (2008).
 - [15] A. S. Kheifets and I. A. Ivanov, “Delay in atomic photoionization,” *Phys. Rev. Lett.* **105**, 233002 (2010).
 - [16] Michael Klaiber, Enderalp Yakaboylu, Heiko Bauke, Karen Z. Hatsagortsyan, and Christoph H. Keitel, “Under-the-barrier dynamics in laser-induced relativistic tunneling,” *Phys. Rev. Lett.* **110**, 153004 (2013).
 - [17] Jing Zhao and Manfred Lein, “Determination of ionization and tunneling times in high-order harmonic generation,” *Phys. Rev. Lett.* **111**, 043901 (2013).
 - [18] C. R. McDonald, G. Orlando, G. Vampa, and T. Brabec, “Tunnel ionization dynamics of bound systems in laser fields: How long does it take for a bound electron to tunnel?” *Phys. Rev. Lett.* **111**, 090405 (2013).
 - [19] Enderalp Yakaboylu, Michael Klaiber, Heiko Bauke, Karen Z. Hatsagortsyan, and Christoph H. Keitel, “Relativistic features and time delay of laser-induced tunnel ionization,” *Phys. Rev. A* **88**, 063421–063442 (2013).
 - [20] Enderalp Yakaboylu, Michael Klaiber, and Karen Z. Hatsagortsyan, “Wigner time delay for tunneling ionization via the electron propagator,” *Phys. Rev. A* **90**, 012116 (2014).
 - [21] G. Orlando, C. R. McDonald, N. H. Protik, G. Vampa, and T. Brabec, “Tunnelling time, what does it mean?” *J. Phys. B: At., Mol. Opt. Phys.* **47**, 204002 (2014).
 - [22] Alexandra S. Landsman, Matthias Weger, Jochen Maurer, Robert Boge, André Ludwig, Sebastian Heuser, Claudio Cirelli, Lukas Gallmann, and Ursula Keller, “Ultrafast resolution of tunneling delay time,” *Optica* **1**, 343 (2014).
 - [23] Michael Klaiber, Karen Z. Hatsagortsyan, and Christoph H. Keitel, “Tunneling dynamics in multiphoton ionization and attoclock calibration,” *Phys. Rev. Lett.* **114**, 083001 (2015).
 - [24] Lisa Torlina, Felipe Morales, Jivesh Kaushal, Igor Ivanov, Anatoli Kheifets, Alejandro Zielinski, Armin Scrinzi, Harm Geert Muller, Suren Sukiasyan, Misha Ivanov, and Olga Smirnova, “Interpreting attoclock measurements of tunnelling times,” *Nat. Phys.* **11**, 503–508 (2015).
 - [25] I. A. Ivanov and Kyung Taec Kim, “Relativistic approach to the tunneling-time problem,” *Phys. Rev. A* **92**, 053418 (2015).

- [26] Alexandra S. Landsman and Ursula Keller, “Attosecond science and the tunnelling time problem,” *Phys. Rep.* **547**, 1–24 (2015).
- [27] Nicolas Teeny, Enderalp Yakaboylu, Heiko Bauke, and Christoph H. Keitel, “Ionization time and exit momentum in strong-field tunnel ionization,” *Phys. Rev. Lett.* **116**, 063003 (2016).
- [28] Alfred Maquet, Jérémie Caillat, and Richard Taïeb, “Attosecond delays in photoionization: time and quantum mechanics,” *J. Phys. B: At., Mol. Opt. Phys.* **47**, 204004 (2014).
- [29] T. F. Gallagher, “Above-threshold ionization in low-frequency limit,” *Phys. Rev. Lett.* **61**, 2304–2307 (1988).
- [30] P. B. Corkum, N. H. Burnett, and F. Brunel, “Above-threshold ionization in the long-wavelength limit,” *Phys. Rev. Lett.* **62**, 1259–1262 (1989).
- [31] P. B. Corkum, “Plasma perspective on strong field multiphoton ionization,” *Phys. Rev. Lett.* **71**, 1994–1997 (1993).
- [32] K. J. Schafer, Baorui Yang, L. F. DiMauro, and K. C. Kulander, “Above threshold ionization beyond the high harmonic cutoff,” *Phys. Rev. Lett.* **70**, 1599–1602 (1993).
- [33] Jivesh Kaushal and Olga Smirnova, “Nonadiabatic Coulomb effects in strong-field ionization in circularly polarized laser fields,” *Phys. Rev. A* **88**, 013421 (2013).
- [34] Bernold Feuerstein and Uwe Thumm, “On the computation of momentum distributions within wavepacket propagation calculations,” *J. Phys. B: At., Mol. Opt. Phys.* **36**, 707–716 (2003).
- [35] Xu Wang, Justin Tian, and J. H. Eberly, “Extended virtual detector theory for strong-field atomic ionization,” *Phys. Rev. Lett.* **110**, 243001 (2013).
- [36] X. O. Pladevall and J. Mompart, *Applied Bohmian Mechanics: From Nanoscale Systems to Cosmology* (Pan Stanford, Singapore, 2012).
- [37] Gregory Lantoine and Ryan P. Russell, “Complete closed-form solutions of the Stark problem,” *Celestial Mechanics and Dynamical Astronomy* **333–366**, 333–366 (2011).
- [38] Tsuneya Ando, Alan B. Fowler, and Frank Stern, “Electronic properties of two-dimensional systems,” *Rev. Mod. Phys.* **54**, 437–672 (1982).
- [39] Kazuyoshi Tanaka, Masahiro Kobashi, Tokushige Shichiri, Tokio Yamabe, David M. Silver, and Harris J. Silverstone, “Losurdo-stark effect for a hydrogenic impurity in a thin layer: Two-dimensional model,” *Phys. Rev. B* **35**, 2513–2516 (1987).
- [40] S. Glutsch, D. S. Chemla, and F. Bechstedt, “Numerical calculation of the optical absorption in semiconductor quantum structures,” *Phys. Rev. B* **54**, 11592–11601 (1996).
- [41] Adrian N. Pfeiffer, Claudio Cirelli, Mathias Smolarski, Darko Dimitrovski, Abu-samha Mahmoud, Lars Bojer Madsen, and Ursula Keller, “Attoclock reveals natural coordinates of the laser-induced tunnelling current flow in atoms,” *Nat. Phys.* **8**, 76–80 (2011).
- [42] Tae Jun Park and J. C. Light, “Unitary quantum time evolution by iterative Lanczos reduction,” *J. Chem. Phys.* **85**, 5870 (1986).
- [43] Randolph Beerwerth and Heiko Bauke, “Krylov subspace methods for the Dirac equation,” *Comp. Phys. Comm.* **188**, 189–197 (2015).
- [44] P. Ehrenfest, “Bemerkung Über die angenäherte Gültigkeit der klassischen Mechanik innerhalb der Quantenmechanik,” *Z. Physik* **45**, 455–457 (1927).
- [45] X. L. Yang, S. H. Guo, F. T. Chan, K. W. Wong, and W. Y. Ching, “Analytic solution of a two-dimensional hydrogen atom. I. Nonrelativistic theory,” *Phys. Rev. A* **43**, 1186–1196 (1991).
- [46] Vincenzo Aquilanti, Simonetta Cavalli, and Cecilia Coletti, “The d -dimensional hydrogen atom: hyperspherical harmonics as momentum space orbitals and alternative sturmian basis sets,” *Chemical Physics* **214**, 1–13 (1997).
- [47] L. Sælen, R. Nepstad, J. P. Hansen, and L. B. Madsen, “The N -dimensional Coulomb problem: Stark effect in hyperparabolic and hyperspherical coordinates,” *J. Phys. A: Math. Theor.* **40**, 1097–1104 (2007).
- [48] L. D. Landau and E. M. Lifshitz, *Quantum Mechanics: Non-relativistic Theory* (Butterworth-Heinemann, Oxford, 1977).
- [49] G. B. Arfken and H. J. Weber, *Mathematical Methods for Physicists* (Academic Press, Oxford, 2013).